Open Access Articles

Fatigue Crack Growth Mechanisms for Nickel-based Superalloy Haynes 282 at 550-750° C

Oregon State
UNIVERSITY

Fatigue Crack Growth Mechanisms for Nickel-based Superalloy Haynes 282 at 550-750 °C

Kyle A. Rozman, Jamie J. Kruzic, John S. Sears, and Jeffrey A. Hawk

The fatigue crack growth rates for nickel-based superalloy Haynes 282 were measured at 550, 650, and 750 °C using compact tension specimens with a load ratio of 0.1 and cyclic loading frequencies of 25 and 0.25 Hz. The crack path was observed to be primarily transgranular for all temperatures, and the observed effect of increasing temperature was to increase the fatigue crack growth rates. The activation energy associated with the increasing crack growth rates over these three temperatures was calculated less than 60 kJ/mol, which is significantly lower than typical creep or oxidation mechanisms; therefore, creep and oxidation cannot explain the increase in fatigue crack growth rates. Transmission electron microscopy was done on selected samples removed from the cyclic plastic zone, and a trend of decreasing dislocation density was observed with increasing temperature. Accordingly, the trend of increasing crack growth rates with increasing temperature was attributed to softening associated with thermally assisted cross slip and dislocation annihilation.

	Symbols
ΔK	Stress intensity range
R	Load ratio
da/dN	Fatigue crack growth rate
$k_{FCP} f(a)$	A term containing all non-temperature-dependent terms related to fracture mechanics (i.e., stress intensity range, load ratio, yield strength, crack length, etc.)
Q	Apparent activation energy
R_g	Universal gas constant
T	Temperature
N	Normalization factor
W	Compact tension specimen width
B	Compact tension specimen thickness
F	Frequency

1. Introduction

With service conditions of the next generation advanced ultra-supercritical (A-USC) steam turbines calling for 100,000 h lifetimes in steam environments where temperatures and pressures are in excess of 760 °C and 35 MPa (Ref 1), it is imperative to investigate fatigue failure mechanisms for potential rotor alloys. Especially important is the effect of creep on fatigue crack growth. At high temperatures ($T > 0.3\ T_{melt}$), thermally activated, time-dependent, mechanisms may influence mechanical properties. With a melting range around 1300 °C for nickel-based superalloys targeted for A-USC turbine rotors, service conditions call for homologous temperatures up to $T/T_{melt} \approx 0.66$. In A-USC turbine applications, time-dependent visco-plastic creep damage and oxidation damage are both significant concerns. Creep may affect the fatigue crack growth mechanism in three ways: (i) microstructural changes (i.e., precipitate coarsening, chemical diffusion), (ii) stress relaxation (i.e., diffusion enhanced dislocation motion), and (iii) creep crack growth (i.e., nucleation and coalescence of vacancies ahead of a growing crack). Similarly, oxidation may affect the fatigue crack growth via mechanisms such as stress-assisted grain boundary oxidation or embrittlement (Ref 2). Either situation may lead to the local microstructure ahead of the crack tip

changing during exposure at A-USC temperatures and pressures, potentially changing the fatigue crack propagation behavior.

Previously, Rozman et al. (Ref 3) reported on the fatigue crack growth rate (da/dN) behavior of nickel-based superalloy Haynes 282, which is a candidate alloy for use in A-USC steam turbines. It was found that when temperature was increased from 550 to 750 °C da/dN increased by ~20 to 60% dependent on applied stress intensity level. While the fracture surfaces showed transgranular crack growth, at 750 °C, there were occasional local excursions onto an intergranular crack path, especially at 0.25 Hz. The purpose of the present paper is to combine new TEM results with an analysis of the activation energy to better understand the possible thermally activated mechanisms that may be responsible for the enhanced fatigue growth rates seen in Haynes 282 with increasing temperature.

2. Materials and Method

2.1 Material

Table 1 shows the nominal chemical composition for Haynes 282 (Ref 4, 5). A rolled plate of Haynes 282 was

Kyle A. Rozman, ORISE, National Energy Technology Laboratory, 1450 Queen Avenue S.W., Albany, OR 97321; Jamie J. Kruzic, Materials Science, School of Mechanical, Industrial, and Manufacturing Engineering, Oregon State University, Corvallis, OR 97331; John S. Sears, AECOM, National Energy Technology Laboratory, 1450 Queen Avenue SW, Albany, OR 97321 and National Energy Technology Laboratory, 1450 Queen Avenue S.W., Albany, OR 97321; and Jeffrey A. Hawk, National Energy Technology Laboratory, 1450 Queen Avenue S.W., Albany, OR 97321. Contact e-mail: jeffhawk4@comcast.net.

obtained from Haynes International in the solution annealed condition with dimensions 333 mm × 254 mm × 35 mm, and the actual composition is also shown in Table 1 (Ref 6). The plate was heat treated in the following manner: (1) solutionizing at >1175 °C for 1 h, followed by (2) cooling to near room temperature, at which point the plate was returned to the furnace for the precipitation aging sequence. The plate was then (3) aged at 1010 °C for 2 h (commensurate with plate thickness) before being air cooled to below 788 °C. It was then (4) returned to the furnace at 788 °C for an additional 8 h exposure to fully develop the γ' precipitates. The plate was removed from the furnace and (5) air cooled to room temperature. This is the standard heat treatment suggested by the manufacturer for Haynes 282 in order to develop peak tensile strength.

Figure 1 shows the general microstructure of peak-aged Haynes 282 that was tested in this research study. In this figure, diffraction pattern A shows matrix ⟨100⟩ orientation with γ' superlattice reflections as well as reflections from the carbide. In diffraction pattern B, also ⟨100⟩ orientation, the lattice matrix reflections and those associated with γ' are seen. The peak-aged microstructure of the plate had an American ASTM grain size of 4 (∼90 μm grain size) (Ref 3). The γ' precipitates were observed by TEM to be between ∼20 and 50 nm in diameter (Ref 3). No secondary or tertiary γ' precipitates were seen in the samples tested in this research. Abundant twins are observed in the peak-aged microstructure with Cr-Mo carbides of the $M_{23}C_6$-type decorating the twin boundaries and termination points.

Figure 2 shows another area from a peak-aged specimen of Haynes 282. In this image, a twin is seen in the left-hand micrograph. In the right-hand micrograph, higher magnification, very fine carbide is found along the twin boundary. Where the twin abuts against the adjacent grain through a high-angle grain boundary, the carbide is much larger. This is typical of primary carbide formed during solidification prior to thermo-mechanical processing, solution heat treatment, and aging, and then coarsened through each subsequent processing and heat treatment step. The carbide along the twin interface probably nucleated and grew as a consequence of thermo-mechanical processing and subsequent heat treatment once the twin formed. Note, Fig. 2 shows the microstructure that existed prior to any mechanical testing.

Shown in the graph (Fig. 3) is the change in yield stress and tensile strength with temperature for Haynes 282 (Ref 4-6). Haynes 282 has relatively constant yield stress up to 800 °C with the yield stress dropping by approximately 12% from room temperature through 760 °C. From 550 to 750 °C (i.e., the temperature range of testing in this study), yield stress is fairly uniform and constant. Ductility for Haynes 282 is also very good (>20% elongation) at all test temperatures (Ref 5, 6).

2.2 Experimental Procedures

Full details of the fatigue crack growth experimental setup and testing procedure are described elsewhere (Ref 3, 7) and only a brief synopsis will be given here. Fatigue crack growth experiments were done in general accordance with ASTM Standard E647 (Ref 8). Compact tension, C(T), specimens were machined from the peak-aged plate in the short transverse direction with the following nominal dimensions: width (W) equal to 25.4 mm and thickness (B) equal to 6.4 mm. Temperatures chosen for fatigue crack growth rate testing were 550, 650, and 750 °C. Testing was conducted using 25 Hz sine wave loading and 0.25 Hz triangle wave loading with a ratio of minimum to maximum load, i.e., $R = P_{min}/P_{max}$, equal to 0.1. The triangular waveform gives constant stain rate which is the more desirable loading condition. However, the triangle waveform is not achievable at 25 Hz, in which case the sinusoidal waveform was selected. From Fig. 2, it can be seen that the temperature range used for fatigue crack growth testing corresponds to a fairly constant yield strength, while tensile strength begins to decrease sharply above 700 °C.

Analysis of the crack growth rates at three temperatures was conducted to determine the activation energy, Q, for fatigue crack growth. In order to calculate Q, the rate of crack growth
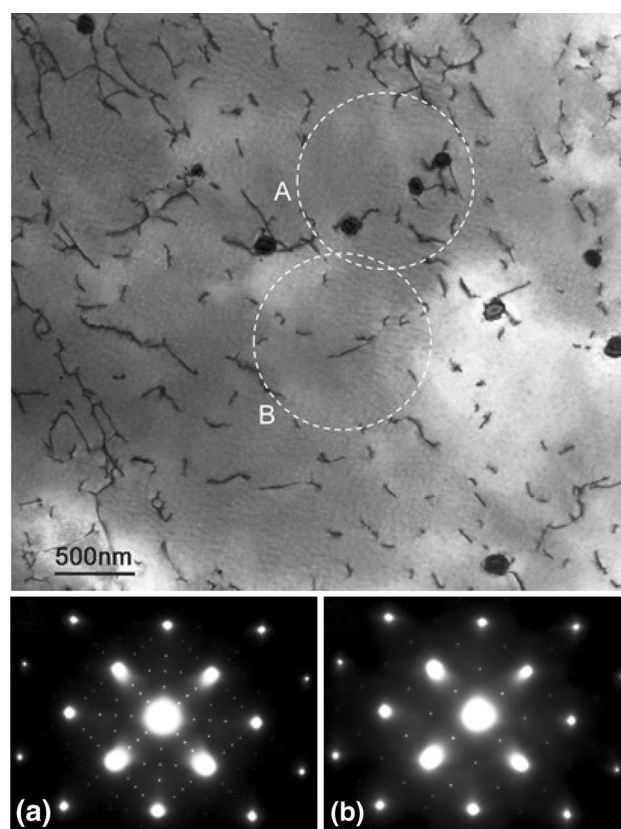

Fig. 1 Microstructure of Haynes 282 in peak-aged state showing dislocations, carbide particles, and gamma prime. Diffraction pattern (a) is from a region containing matrix, gamma prime, and carbide (note extra reflections from carbide), and (b) is the diffraction pattern from matrix and gamma prime only

Table 1 Nominal and actual chemical composition (wt.%) of Haynes 282 (Ref 4, 6)

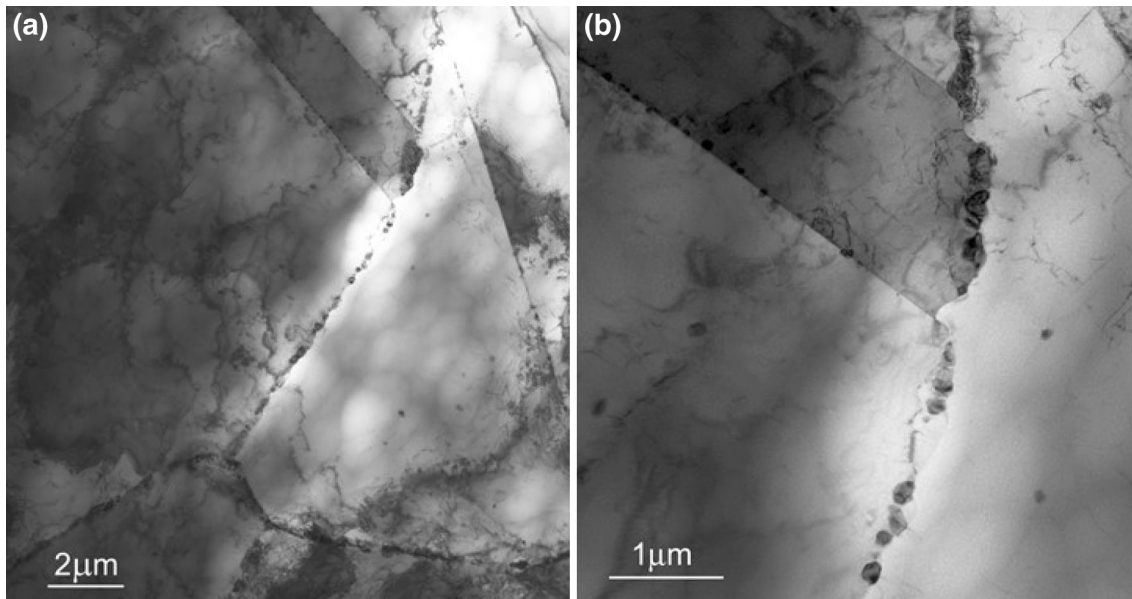| H282	Ni	Cr	Co	Mo	Ti	Al	Fe	Mn	Si	C	B
Nominal	Bal	19.5	10	8.5	2.1	1.5	1.5	0.3	0.15	0.06	0.005
Actual	Bal	19.62	10.36	8.56	2.19	1.45	0.4	0.08	0.05	0.067	0.004

Fig. 2 Microstructure of Haynes 282 in peak-aged state showing (a) low magnification image of grain boundaries with carbide and twins; and (b) a higher magnification image of the twin showing fine carbide along one edge of the twin interface and much larger carbide where it butts against an adjacent matrix grain
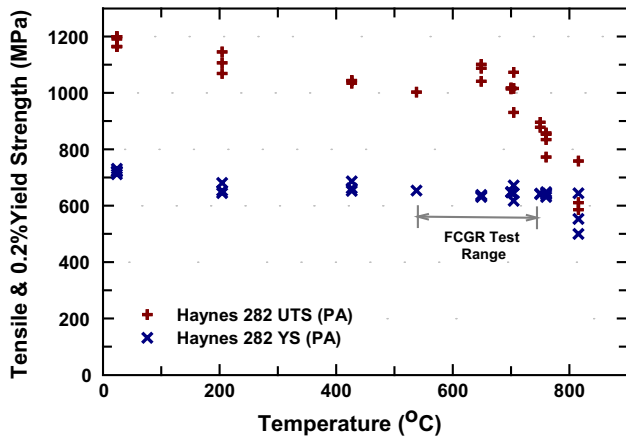

Fig. 3 Yield stress and tensile strength for peak-aged (PA) Haynes 282 as a function of test temperature (Reproduced from data contained in (Ref 6)

was assumed to be proportional to an Arrhenius relationship typical of solid-state reactions (Ref 9-12). Equation 1 was proposed by Starink and Reed (Ref 13) specifically for fatigue crack propagation.

$$\frac{da}{dN} \alpha k_{\text{FCP}} f(a) \exp\left(\frac{-Q}{R_g T}\right). \quad (\text{Eq 1})$$

In Eq 1, da/dN is the fatigue crack growth rate; $k_{\text{FCP}} f(a)$ is a term containing all non-temperature-dependent terms (e.g., stress intensity range, load ratio, yield strength, crack length, etc.); Q is the apparent activation energy for crack growth; R_g is the universal gas constant; and T is the temperature.

In this study, activation energies were calculated at integer values of the stress intensity range, ΔK, from previously published fatigue crack growth data (Ref 3), which are shown in Fig. 3 as a function of test frequency at each test temperature. At each ΔK, the average da/dN was plotted

against the inverse of temperature, $1/T$. The slope of a linear fit of each curve corresponds to the apparent activation energy for fatigue crack growth for a specific ΔK. Uncertainty was calculated from residuals of the linear regression analyses.

Fracture surfaces were investigated using a scanning electron microscope (FEI, Inspect F) in secondary electron imaging mode. In order to estimate the applied stress intensity range represented in the fractographic image, the position on each image was recorded and correlated to the applied ΔK from the corresponding test using the end of the precrack as the index point.

The microstructure in the cyclic plastic zones for six samples was investigated by transmission electron microscopy (TEM) using a Philips/FEI CM200 STEM. First fatigue crack growth specimens were prepared by growing at constant stress intensity range for a minimum of 2 mm. The applied ΔK was maintained constant at $\Delta K = 9.0 \pm 0.1$ MPa√m at 25 Hz, while for 0.25 Hz loading frequency, ΔK was maintained constant at $\Delta K = 14.6 \pm 0.1$ MPa√m. The higher ΔK level was used for 0.25 Hz to keep the experimental time to grow 2 mm reasonable (<20 h). Specimens for the TEM were then fabricated by the focused ion beam (FIB) lift-out method using an FEI Quanta 3D FEG dual beam microscope. Sample extraction for TEM specimens was selected inside the plastic zone, with orientation roughly parallel to the crack path, i.e., the plane of the TEM sample was coplanar with the crack path. The TEM specimens measured approximately 7 μm × 7 μm. Thickness was not measured; however, thickness was estimated around ~50 nm for electron transparency.

3. Results

3.1 Fatigue Crack Growth Rates and Fractography for Haynes 282

Figure 4 shows the measured crack growth rate (da/dN) as a function of the applied ΔK for Haynes 282 at 550, 650, and
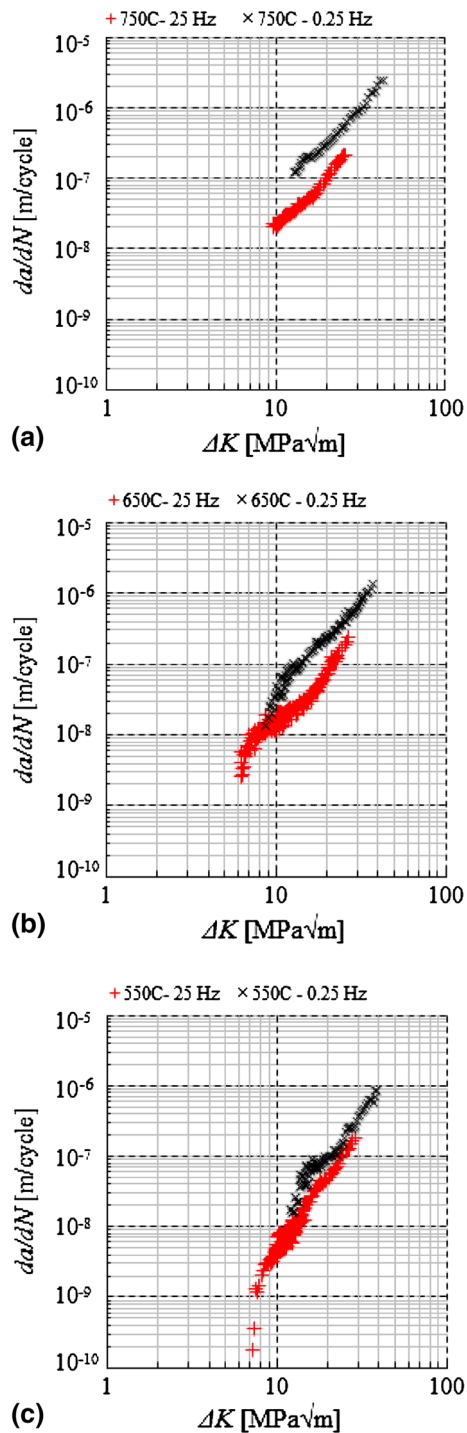
Fig. 4 Fatigue crack growth rates of Haynes 282 with load ratio 0.1 at 25 and 0.25 Hz (Ref 3, 7): (a) At 750 °C; (b) At 650 °C; (c) At 550 °C

750 °C at the two test frequencies. Note that at 25 Hz, loading of the compact tension specimen was done with a sine wave, while at 0.25 Hz loading was accomplished using a triangular waveform. The effect of increasing temperature on fatigue crack growth rate was to increase da/dN at a given applied ΔK (Ref 3). Frequency also increased da/dN at a given applied ΔK (Fig. 3). The frequency effect was more pronounced at 650 and 750 than at 550 °C.

As noted by Rozman et al. (Ref 3), inspection of the fracture surfaces showed that crack growth occurred in a transgranular manner. However, there were some small and localized intergranular features on the fracture surfaces for those $C(T)$ specimens tested at 750 °C. For fatigue crack growth tests at 25 Hz loading frequency, intergranular features were isolated to a single grain facet (Ref 3) and were only present for $\Delta K < 11$ MPa√m. At 0.25 Hz loading frequency intergranular features persisted at all ΔK levels. Sometimes these features were clustered together at lower ΔK (Fig. 5a), while at higher ΔK, intergranular crack growth features typically encompassed a single grain (Fig. 5b).

Preliminary testing at 0.05 Hz loading frequency was also done. After the ASTM specified fatigue crack growth tests were completed, approximately 2 to 4 mm of uncracked specimen remained. To break the sample in half for fractographic analysis, the $C(T)$ specimen was loaded at 0.05 Hz at 650 and 750 °C in constant load mode. While this test was not ASTM valid (i.e., edge effects are expected as the plastic zone size exceeded the physical sample size), the intent was to see if the crack path, and thus, the fracture mode, would transition to fully intergranular. At 650 °C, the crack growth mode stayed fully transgranular, while at 750 °C, intergranular features were once again found in isolated locations on the fracture surface, and often these features were clustered even at high ΔK levels (Fig. 6).

3.2 Apparent Activation Energy

Figure 7 shows apparent activation energies correlated to an average ΔK level from the testing done in this research. Apparent activation energy was calculated by a linear fit of inverse temperature versus crack growth rate (Eq 1). Uncertainty in activation energy (i.e., error bars in Fig. 7) was estimated as the standard error of the linear fit, which ranged from a high of 30% to a low of 3%. The average uncertainty in activation energy at 25 Hz loading frequency was ∼15%, while at 0.25 Hz, it was ∼17% (Ref 7).

Apparent activation energy, Q, is correlated to a ΔK value at 25 Hz loading frequency in Fig. 7(a), while similar results are shown in Fig. 7(b) for the 0.25 Hz loading frequency. Crack growth rates from each temperature and ΔK level were taken from an average of three data points (minimum), and the uncertainty in the calculations is represented by the error bars. The apparent activation energy decreases as ΔK increases, which indicates da/dN is less temperature dependent at higher ΔK values. Linear regression analyses indicated this trend is significant at both frequencies ($p < 0.05$).

3.3 Cyclic Plastic Zone Microstructure

Bright-field TEM of the microstructures in the plastic zone ahead of the crack tip at each test temperature is presented in Fig. 8 for the 0.25 Hz test frequency. Similar observations to the 0.25 Hz microstructure were made at 25 Hz. Only the 0.25 Hz microstructure is presented. Dislocation density was very high at 550 °C (Fig. 7a). At 650 °C and 750 °C, the dislocation density was qualitatively lower as it was not possible to resolve individual dislocations to calculate a density. However, individual dislocations were more easily seen at 750 °C (Fig. 7c). As previously stated, no attempt was made to determine dislocation densities in these samples (at this time) because TEM specimen preparation through FIB approach did not generate sufficient electron-transparent material for suffi-
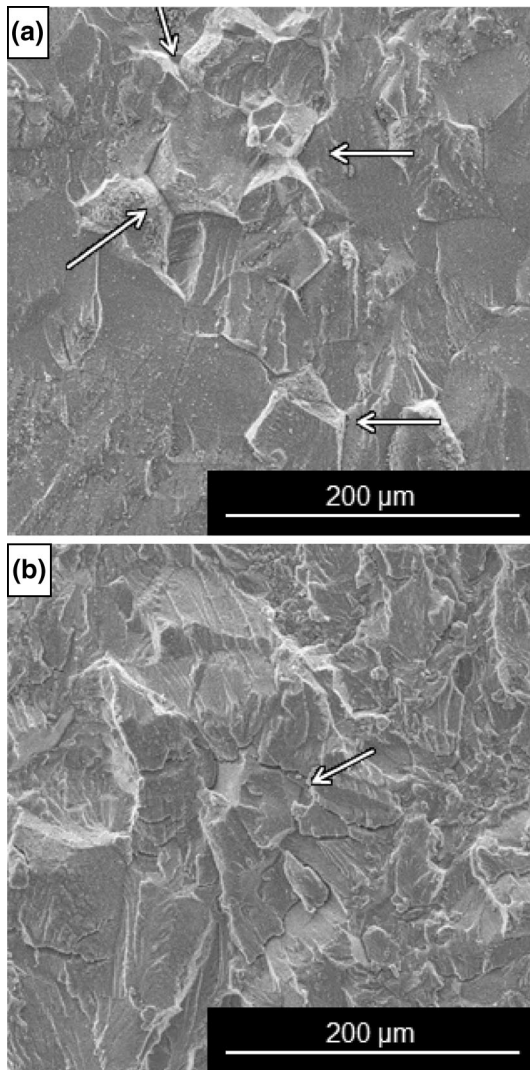
Fig. 5 Some isolated intergranular features observed during crack growth at 750 °C at various testing frequencies and ΔK (Ref 7). (a) Showing intergranular features clustered in one area, with experimental conditions of T = 750 °C, f = 0.25 Hz, ΔK = 14 MPa√m; (b) Showing intergranular features limited to a single grain, with experimental conditions of T = 750 °C, f = 0.25 Hz, ΔK = 33 MPa√m

cient specimen tilting to different crystallographic orientations. However, what is very clear is the level of deformation that occurs in the plastic zone ahead of the growing crack. Referencing Fig. 1 and 2, it is clear to see the tremendous change in the general features of the Haynes 282 microstructure in the plastic zone ahead of the crack after terminating the test. All feature details relative to twins, grains, γ′ and carbides are obscured by the high density of dislocations and the strain from their interaction with each other, especially at 550 °C, and to a somewhat lesser extent at 650 and 750 °C. In Fig. 7(c), it is possible to image individual dislocations and there are indications for certain ones being influenced by γ′ during deformation. Additional TEM was performed on selected FIB's specimens utilizing a new ion polishing system at low kV, in an attempt to increase the amount of electron-transparent material without introducing additional damage from the ion beam. Those results will be reported in a subsequent paper but those observations support the general microstructure features noted herein.
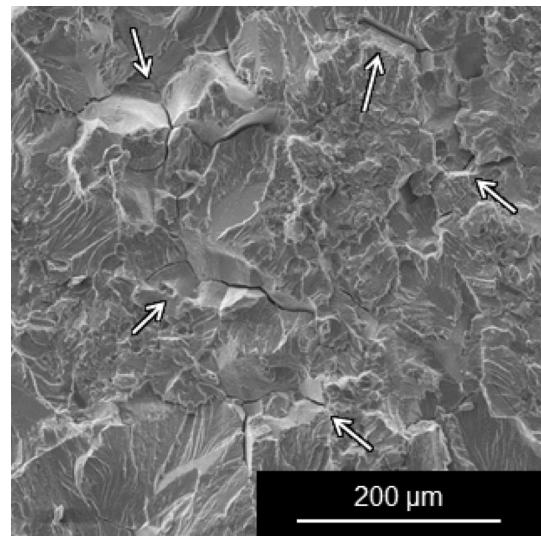

Fig. 6 Showing large cluster of intergranular features, with experimental conditions of T = 750 °C, f = 0.05 Hz, ΔK = 40 MPa√m

4. Discussion

4.1 Apparent Activation Energy for Fatigue Crack Growth

Understanding the thermally activated mechanisms involved in fatigue crack growth is important to define appropriate service conditions for the alloy and aid the development of new alloys. While post-failure fractography can easily identify primary modes of fatigue crack growth (i.e., transgranular or intergranular, stage I or II), fractography alone does not always elucidate the reasons why a certain crack propagation mode is observed or why the growth rate increases with temperature. One method to help determine the influence of various failure mechanisms is to compare the apparent activation energy of the crack growth to activation energies for various thermally activated processes such as creep and oxidation.

Based on the calculated activation energies in Fig. 7, a normalization factor was estimated and applied to the fatigue crack growth data in a manner analogous to a Zener-Hollomon approach for creep (Ref 14). The Zener-Hollomon analysis as applied here to da/dN involves multiplying the crack growth rates by a normalization factor (Eq 2) in order to collapse most (if not all) of the data onto a single curve:

$$N = \exp\left(Q/R_{\mathrm{g}}T\right), \qquad \text{(Eq 2)}$$

In Eq 2, N is the normalization factor; Q is the apparent activation energy for fatigue crack growth rate; R_{g} is the universal gas constant; and T is the temperature.

In Fig. 9(a), an activation energy equal to 25 kJ/mol was selected for tests performed at 25 Hz loading frequency, and an activation energy equal to 35 kJ/mol was selected for 0.25 Hz loading frequency Fig. 9(b). Collapse of the fatigue crack growth curves in the Paris law regime suggests that mechanism with apparent activation energy approximately equal to 25 or 35 kJ/mol operates at 25 and 0.25 Hz, respectively, for the specific experimental conditions in this research on Haynes 282. These values of nominal apparent activation energy will be subsequently used in the following sections to discuss the possible temperature dependence of fatigue crack growth
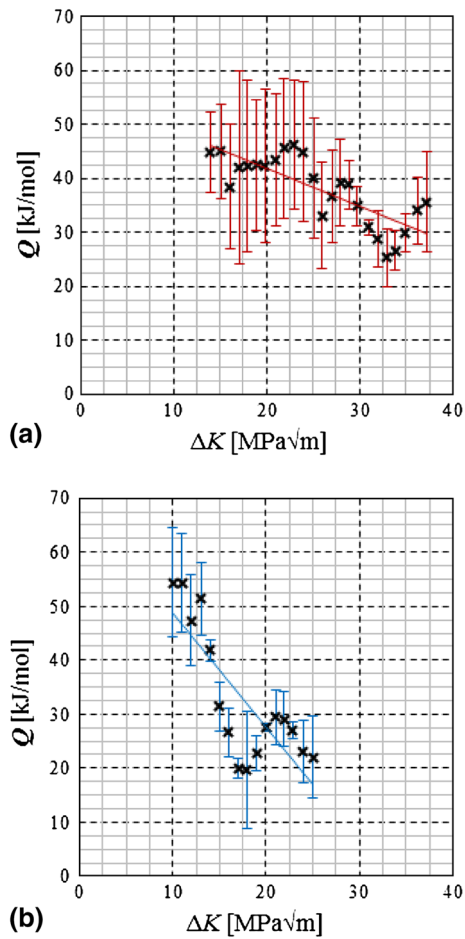
Fig. 7 Apparent activation energy correlated to ΔK for da/dN of Haynes 282 from 550 to 750 °C (Ref 7). Error bars indicate experimental uncertainty. Solid line shows statistically significant linear fit; (a) 0.25 Hz loading frequency and (b) 25 Hz loading frequency

mechanisms for Haynes 282 in the range of temperatures relevant to A-USC steam turbine rotors.

4.2 Oxidation Effects

The effect of increasing test temperature in air was to increase da/dN. Since controlled oxygen partial pressure testing was not conducted, the effect of oxygen must be inferred. Generally, when accelerated fatigue crack growth rates are attributed to oxidation effects in nickel-based superalloys, the resulting crack path is intergranular (Ref 15-19). In this study, intergranular features on the fracture surface were very rare and only present at 750 °C (Fig. 5). There was no observed major shift from the generally transgranular nature of cracking over the range of 550 to 750 °C (Ref 3). The lack of intergranular fracture features suggests that the increase in da/dN is not due to oxidation. This can be further confirmed by looking at the calculated activation energies for oxidation.

From Arrhenius regression of the oxidation data (Table 2) as reported from Pike (Ref 4), the activation energy due to oxidation can be estimated at around 120 kJ/mol, or an oxidation rate very near to that of pure Ni (130 kJ/mol (Ref 20)). With the measured apparent activation energy nominally
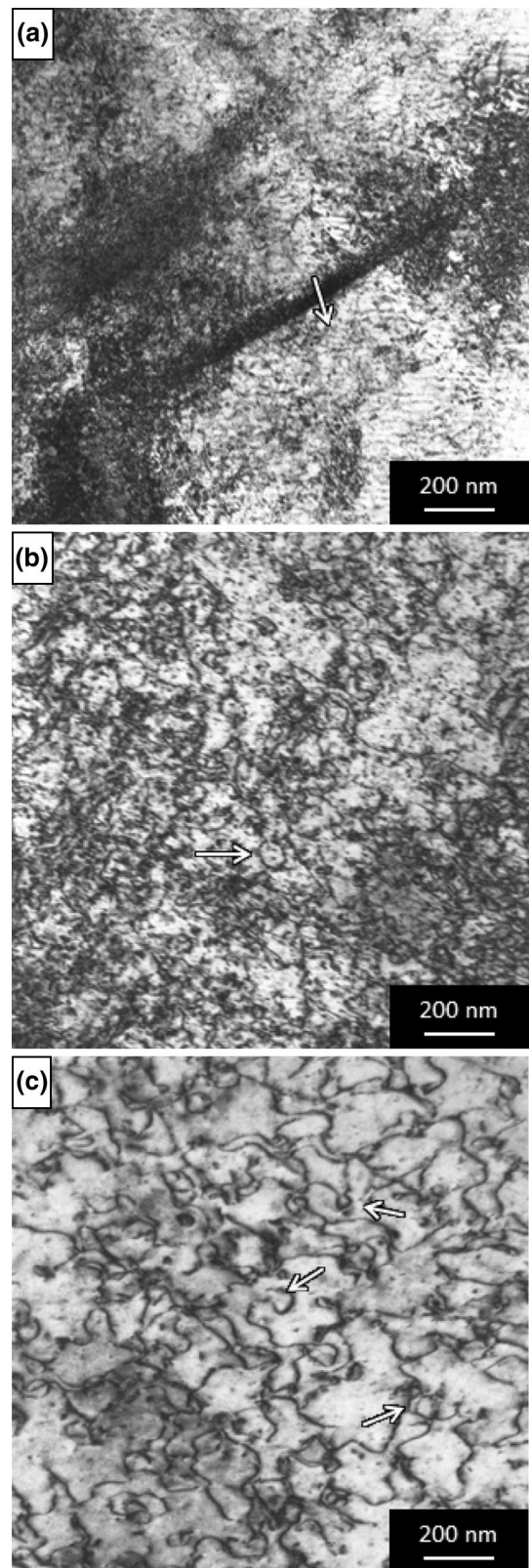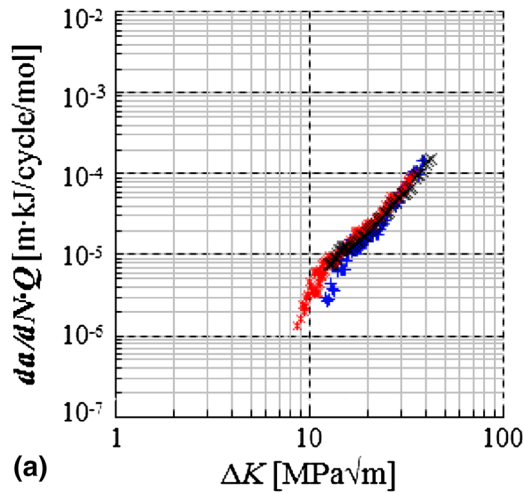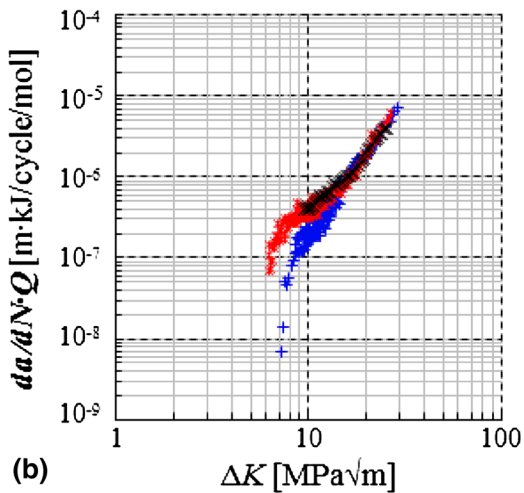

Fig. 8 Transmission electron microscopy bright-field images of the microstructure (Ref 7). Samples were cracked at ΔK of 14.7 MPa√m for a minimum of 2 mm at 0.25 Hz loading frequency. (a) Vein structure at 550 °C, (b) Orowan looping at 650 °C and (c) Orowan looping at 750 °C

+550℃ @ 0.25Hz ∗650℃ @ 0.25Hz ×750℃ @ 0.25Hz

(a)

+550℃ @ 25Hz ∗650℃ @ 25Hz ×750℃ @ 25Hz

(b)

Fig. 9 Normalized fatigue crack growth rates using Zener-Hollomon method (Ref [7]): (a) With apparent activation energy of 35 kJ/mol used at 0.25 Hz; and (b) With apparent activation energy of 25 kJ/mol used at 25 Hz

between 25 and 35 kJ/mol (depending on frequency), and peaking at around 50 kJ/mol, oxidation is not considered to cause the increase in da/dN observed in Haynes 282 with increasing temperature.

4.3 Creep Effects

Review of the literature has indicated that application of a hold time during fatigue tests can significantly increase da/dN (Ref [15], [21-23]). The literature suggests that creep effects are not active until the temperature exceeds 550 °C in various precipitate-hardened nickel-based superalloys (Ref [15], [21]). With an experimentally observed increase in da/dN at lower testing frequencies, and with temperatures at 550 °C, or greater, creep may explain the increase in rate of fatigue crack propagation.

Visual signs of creep may include an intergranular crack path with cavitation along grain boundaries (Ref [24]) or sliding

Table 2 Oxidation depth in Haynes 282 (Ref [4], [5])

Temperature, °C	Depth of oxidation, μm
871	15
927	28
982	46

of grain boundaries (Ref [22]). In contrast, the observed fracture surfaces were generally transgranular. Evidence of grain boundary sliding was found to be indeterminate at this time for the fatigue crack growth rate testing done in this research.

Other creep mechanisms in γ' particle-strengthened alloys like Haynes 282 operate by self-diffusion, dislocation climb, and Orowan looping. The activation energy for climb is the same as that for self-diffusion, which in the case of nickel is 285 kJ/mol (Ref [25], [26]). Again, this value of activation energy is much higher than the apparent activation energy calculated from da/dN for Haynes 282 from current experimental conditions. Thus, based on the observed fractography and activation energies for tests at these temperatures, creep cannot be considered as a significant mechanism.

4.4 Dislocation Interactions

Since the activation energy associated with climb is much higher than was measured, dislocation annihilation by climb cannot account for the decreasing dislocation density with increasing temperature. Rather, dynamic recovery and dislocation annihilation by other means appear to be the most likely cause in reducing the dislocation density as the test temperature increases. The spontaneous annihilation of screw dislocations by cross slip is also known to be thermally activated. Indeed, the minimum critical distance for this mechanism to occur increases as temperature increases (Ref [27], [28]). For example, Paus et al. (Ref [29]) reported the critical minimum distance for cross slip annihilation of a screw dislocation pair in pure nickel increased from 51 nm at 20 °C to 116 nm at 477 °C (Ref [30]). Furthermore, Brown (Ref [31]) found, also for pure Ni, the activation energy for jog migration in screw dislocations was 12.5 kJ/mol. The migration of jogs would also reduce the spacing between screw dislocation dipole pairs until the critical minimum distance for cross slip annihilation is met along the dislocation line. Overall, lower activation energy mechanisms associated with thermally activated cross slip mechanisms are more in line with the present observations and may be responsible for the temperature dependence of da/dN (Fig. 4).

5. Conclusion

Mechanisms associated with creep or oxidation were unable to explain the increase in fatigue crack growth rates with increasing temperature. Fractography revealed that failure occurred transgranularly at all test temperatures, and the apparent activation energies associated with the fatigue crack growth tests were estimated to be on the order of ~25-35 kJ/mol, depending on test frequency, which is much lower than is needed for creep or oxidation. Based on the observed dislocation densities and low apparent activation energies, dynamic recovery via thermally activated cross slip and annihilation of screw dislocations may contribute to the

increase in crack growth rates as testing temperature increases. It is recommended that more detailed TEM studies be conducted in the future to fully investigate this possible mechanism.

With the desired operating temperatures of A-USC power systems possibly reaching 760 °C for the high pressure and intermediate pressure turbines (i.e., ~0.66 T_{melt} of Haynes 282), it is essential that all relevant mechanical properties and deformation mechanisms, including fatigue, are well understood in the range of temperatures near this level since the entire disk will not be at 760 °C. This study has shown Haynes 282 is a relatively robust alloy, not subject to detrimental intergranular failure mechanisms in air environments up to 750 °C with loading frequencies as slow as 0.25 Hz as have been seen in other nickel superalloys. Utilization of Haynes 282 at 760 °C in rotating structural components based on the fatigue crack propagation rate, while promising, is cautioned until further information on other failure modes (e.g., creep-fatigue) is acquired.

Acknowledgments

Disclaimer

References

1. P.D. Jablonski, J.A. Hawk, C.J. Cowen, and P.J. Maziasz, Processing of Advanced Cast Alloys for A-USC Steam Turbine Applications, *J. Mater.*, 2012, **64**(2), p 271–279. doi:10.1007/s11837-012-0241-4

2. D.A. Woodford, Gas phase Embrittlement and Time Dependent Cracking of Nickel Based Superalloys, *Energy Mater. Mater. Sci. Eng. Energy Syst.*, 2006, **1**(1), p 59–70. doi:10.1179/174892306X99679

3. K.A. Rozman, J.J. Kruzic, and J.A. Hawk, Fatigue Crack Growth Behavior of Nickel-Base Superalloy Haynes 282 at 550-750 °C, *J. Mater. Eng. Perform.*, 2015, **24**(8), p 2841–2846

4. Pike, L.M. (2006). *Haynes 282 alloy—A New Wrought Superalloy Designed for Improved Creep Strength and Fabricability (#GT2006-91204), ASME Turbo Expo 2006: Power for Land, Sea and Air*. (pp. 1–9). Barcelona, Spain

5. Haynes® International, (2006). Haynes® 282® Alloy. Retrieved from http://www.haynesintl.com/pdf/h3173.pdf. Accessed January 1st 2015

6. Viswanathan, R., Hawk, J.A., Schwant, R.D., Totemeier, T., Goodstine, S., McNally, M., and Allen, D. B. (2009). *Steam Turbine Materials for Ultrasupercritical Coal Power Plants*. pp. 1–535. Independence, OH

7. Rozman, K.A. (2014) *Characterization of High Temperature Fatigue Mechanisms in Haynes 282 Nickel Based Superalloy*. Doctoral dissertation, Oregon State University

8. ASTM Standard E647—11: *Standard Test Method for Measurement of Fatigue Crack Growth Rates*. ASTM International, West Conshohocken, PA. 2011, doi: 10.1520/E0647-13AE01, www.astm.org

9. S. Vyazovkin, Computational Aspects of Kinetic Analysis. Part C. The ICTAC Kinetics Project—The Light at the End of the Tunnel?, *Thermochim. Acta*, 2000, **355**(1–2), p 155–163. doi:10.1016/S0040-6031(00)00445-7

10. M.J. Starink, The Determination of Activation Energy From Linear Heating Rate Experiments: A Comparison of the Accuracy of Conversion Methods, *Thermochim. Acta*, 2003, **404**(1–2), p 163–176. doi:10.1016/S0040-6031(03)00144-8

11. E.J. Mittemeijer, Analysis of the Kinetics of Phase Transformations, *J. Mater. Sci.*, 1992, **27**(15), p 3977–3987. doi:10.1007/BF01105093

12. T.G. Langdon, A Method of Distinguishing Between Diffusion Creep and Harper-Dorn Creep at Low Stress Levels, *Scr. Mater.*, 1996, **35**(6), p 733–737. doi:10.1016/1359-6462(96)00219-9

13. M.J. Starink and P.A.S. Reed, Thermal Activation of Fatigue Crack Growth: Analyzing the Mechanisms of Fatigue Crack Propagation in Superalloys, *Mater. Sci. Eng. A*, 2008, **491**(1–2), p 279–289. doi: 10.1016/j.msea.2008.02.016

14. C. Zener and J.H. Hollomon, Effect of Strain Rate Upon Plastic Flow of Steel, *J. Appl. Phys.*, 1944, **15**(1), p 22–32. doi:10.1063/1.1707363

15. D. Gustafsson, J. Moverare, S. Johansson, M. Hörnqvist, K. Simonsson, S. Sjöström, and B. Sharifimajda, Fatigue Crack Growth Behavior of Inconel 718 with High Temperature Hold Times, *Proc. Eng.*, 2010, **2**, p 1095–1104. doi:10.1016/j.proeng.2010.03.118

16. J.E. King, Fatigue Crack Propagation in Nickel-Base Superalloys—Effects of Microstructure, Load Ratio, and Temperature, *Mater. Sci. Technol.*, 1987, **3**(9), p 750–764. doi:10.1179/026708387790329766

17. E. Andrieu, R. Molins, H. Ghonem, and A. Pineau, Intergranular Crack Tip Oxidation Mechanism in a Nickel-Based Superalloy, *Mater. Sci. Eng. A*, 1992, **154**(1), p 21–28. doi:10.1016/0921-5093(92)90358-8

18. R. Jiang, S. Everitt, M. Lewandowski, N. Gao, and P.A.S. Reed, Grain Size Effects in a Ni-Based Turbine Disc Alloy in the Time and Cycle Dependent Crack Growth Regimes, *Int. J. Fatigue*, 2014, **62**, p 217–227. doi:10.1016/j.ijfatigue.2013.07.014

19. S. Everitt, R. Jiang, N. Gao, M.J. Starink, J.W. Brooks, and P.A.S. Reed, Comparison of Fatigue Crack Propagation Behaviour in Two Gas Turbine Disc Alloys Under Creep-Fatigue Conditions: Evaluating Microstructure, Environment And Temperature Effects, *Mater. Sci. Technol.*, 2013, **29**(7), p 781–787. doi:10.1179/1743284713Y.0000000229

20. R. Peraldi, D. Monceau, and B. Pieraggi, The Nickel, Model Material for the High Temperature Oxidation Studies: First Steps Towards Predictive Modelling, *Revue de Métallurgie*, 2005, **102**(2), p 135–145. doi:10.1051/metal:2005115

21. J. Byrne, Elevated Temperature Fatigue Crack Growth Under Dwell Conditions in Waspaloy, *Int. J. Fatigue*, 1997, **19**(5), p 359–367. doi: 10.1016/S0142-1123(97)00056-X

22. J. Dahal, K. MacIejewski, and H. Ghonem, Loading Frequency and Microstructure Interactions in Intergranular Fatigue Crack Growth in a Disk Ni-Based Superalloy, *Int. J. Fatigue*, 2013, **57**, p 93–102

23. X. Liu, B. Kang, and K.M. Chang, The Effect of Hold-Time on Fatigue Crack Growth Behaviors of WASPALOY Alloy at Elevated Temperature, *Mater. Sci. Eng. A*, 2003, **340**(1–2), p 8–14. doi:10.1016/S0921-5093(02)00074-6

24. A. Saxena, *Nonlinear Fracture Mechanics for Engineers*, CRC Press LLC, Boca Raton, 1998

25. R. Weast, *Handbook of Chemistry and Physics*, 66th ed., CRC Press, Boca Raton, 1985

26. S.K. Sondhi, B.F. Dyson, and M. McLean, Tension-Compression Creep Asymmetry in a Turbine Disc Superalloy: Roles of Internal Stress and Thermal Ageing, *Acta Mater.*, 2004, **52**(7), p 1761–1772. doi:10.1016/j.actamat.2003.12.017

27. T. Rasmussen, T. Vegge, and T. Leffers, Simulation of Structure and Annihilation of Screw Dislocation Dipoles, *Philos. Mag. A*, 2000, **80**(5), p 1273–1290. doi:10.1080/01418610050024585

28. T. Leffers and O.B. Pedersen, The Activation Energy for the fcc Rolling-Texture Transition as Related to the Activation Energy for Cross Slip, *Scr. Mater.*, 2002, **46**(10), p 741–746. doi:10.1016/S1359-6462(02)00065-9

29. P. Pauš, J. Kratochvíl, and M. Beneš, A Dislocation Dynamics Analysis of the Critical Cross-Slip Annihilation Distance and the Cyclic Saturation Stress in fcc Single Crystals at Different Temperatures, *Acta Mater.*, 2013, **61**(20), p 7917–7923. doi:10.1016/j.actamat.2013.09.032

30. B. Tippelt, J. Breitschneider, and P. Hähner, The Dislocation Microstructure of Cyclically Deformed Nickel Single Crystals at Different Temperatures, *Phys. Status Solidi (a)*, 1997, **163**(1), p 11–26

31. L.M. Brown, A Dipole Model for the Cross-Slip of Screw Dislocations in fcc Metals, *Philos. Mag. A*, 2002, **82**(9), p 1691–1711. doi:10.1080/01418610210130976